Available online at www.sciencedirect.com
ScienceDirect
Journal of Sound and Vibration 301 (2007) 635–648
JOURNAL OF SOUND AND VIBRATION
www.elsevier.com/locate/jsvi

Wave propagation in three-coupled periodic structures

Francesco Romeo*, Achille Paolone

Dipartimento di Ingegneria Strutturale e Geotecnica, Università di Roma "La Sapienza", Rome, Italy

Received 8 February 2006; received in revised form 20 September 2006; accepted 17 October 2006
Available online 28 November 2006

Abstract

Free wave propagation patterns for general three-coupled periodic structures are investigated by means of the transfer matrix approach. It is shown that an exhaustive description of the propagation domains requires spaces that are stratified in homogeneous regions, whose dimension is given by the number of invariants of the transfer matrix characteristic equation and whose boundaries are represented by codimension-one manifolds. Three types of three-coupled periodic mechanical models characterized by constitutive elastic and/or inertial coupling between mono- and bi-coupled dynamics, namely pipes, thin-walled beams and truss beams, are considered. From the design standpoint, an adequate representation of the propagation domains pattern is obtained through a nonlinear mapping from the space of the invariants to the physical parameters plane. The analyzed models give rise to equations of motion where the three-coupled nature stems from the coupling between transversal (bi-coupled) and longitudinal (mono-coupled) dynamics for the pipes and truss beams, whilst coupling occurs between transversal and torsional (mono-coupled) dynamics when it comes to the thin-walled beams. A mechanical interpretation associated with the bounding frequencies of the propagation regions is given and the evolution of the propagation properties when coupling parameters tend to vanish is discussed.

1. Introduction

Periodic structures are called *n-coupled* when their modular elements are coupled through n degrees of freedom [1]; in this work, the dynamics of three-coupled periodic structures is analyzed through the single-element transfer matrix properties. The well-known transfer matrix method was also investigated to analyze periodic structures by a number of authors including [2–5] and extended to the so-called wave vector approach in Refs. [6,7]. The latter is based primarily on the diagonalization of the single-element transfer matrix to avoid the numerical difficulties that may arise in the transfer matrices multiplication in case of a large number of periodic elements. The main advantage of relying on transfer matrices lies in the reduction of the dimension of the whole periodic structure problem to $2n$. A number of applications pertaining to multi-coupled periodic structures have been proposed so far. To name but a few, periodic and disordered truss beams were examined in Refs. [5,8–10], generic structural networks in Refs. [6,11] and piecewise periodic structures in Refs. [12,13]. Transfer matrix mathematical insights were also handled in Refs. [14,15]. As shown in Ref. [16], the propagation properties of periodic structures are thoroughly described on spaces with the minimum dimension

*Corresponding author.
E-mail addresses: francesco.romeo@uniroma1.it (F. Romeo), achille.paolone@uniroma1.it (A. Paolone).

0022-460X/$ - see front matter © 2006 Elsevier Ltd. All rights reserved.
doi:10.1016/j.jsv.2006.10.017

necessary to qualitatively characterize the type of eigenvalues. These spaces, whose dimension is given by the number of invariants of the transfer matrix characteristic equation, are stratified in homogeneous regions bounded by codimension-one manifolds. Recently instances of three-coupled periodic mechanical models were also addressed by the authors [17]. In this work, the aforementioned study is extended to determine the bounding manifolds defining pass, stop and complex regions on the space of the invariants of general three-coupled periodic structures. Also, this system-independent representation is specialized to handle three paradigmatic models chosen to represent structures whose three-coupled nature results from different sources. Such models are pipes, characterized by elastic constitutive coupling, thin-walled beams, characterized by inertial constitutive coupling, and truss beams characterized by both of them. Periodic pipes resting on elastic supports, modeled as thin cylindrical shells undergoing axisymmetric (*breathing*) modes of vibration, are considered [18]. Thin-walled beams with symmetric cross-section resting on elastic supports undergoing flexural–torsional oscillations are then analyzed. Finally, truss beams are studied. As far as the latter are concerned, equivalent continuum models were proposed in Refs. [20,21]. According to this approach, being mainly interested to the global dynamic behavior, local periodicity (the single truss module) is studied by using an equivalent continuum model obtained through homogenization techniques [19]. Then, global periodicity (evenly spaced supports) is examined by deriving the transfer matrix. The selected models give rise to equations of motion where the three-coupled nature stems from the coupling between transversal (bi-coupled) and longitudinal (mono-coupled) dynamics for the pipes and truss beams, respectively. For thin-walled beams, by contrast, coupling arises between transversal and torsional (mono-coupled) dynamics. In pipes, the elastic coupling occurs as a result of the Poisson effect; in the equivalent truss models, the inertial coupling is due to both the different cross-sections of top and bottom bars and to the difference between top and bottom nodal mass of the truss module; in thin-walled beams, instead, inertial and elastic coupling occurs whenever the centroid and the flexural center fail to coincide. Consequently, the matching coupling parameters are the Poisson coefficient for pipes, either the relative cross-sections of the top and bottom bars and the relative masses of the top and bottom nodes for the equivalent truss beams, and the distance between the centroid and the flexural center for the thin-walled beams. For each model, the boundaries of the propagation regions are determined in the physical parameters' space. Furthermore, the evolution of the propagation properties is discussed when the coupling parameters tend to vanish, thus leading to uncoupled equations. They correspond to the longitudinal bar and either the beam on a spring bed or the Euler–Bernoulli beam, for the pipes or the equivalent truss beams, respectively; the torsional bar and the Euler–Bernoulli beam for the thin-walled beams. Extending Mead's results a mechanical interpretation of the bounding frequencies of the propagation regions is eventually provided.

2. Propagation regions on the space of the invariants

A generic periodic structure whose elements are coupled through $n = 3$ degrees of freedom to the adjacent ones is considered. The dynamic behavior of these three-coupled structures is properly described by means of the transfer matrix method. Let $\mathbf{z}_k^{\mathrm{T}} = (\mathbf{d}_k^{\mathrm{T}}\mathbf{f}_k^{\mathrm{T}})$ be the state vector of generalized displacement $\mathbf{d}_k$ and forces $\mathbf{f}_k$ at the coupling point k; under the transfer matrix approach, the state vector $\mathbf{z}_{k+1}$ at the coupling point $k+1$ is related to the state vector $\mathbf{z}_k$ by

$$\mathbf{z}_{k+1} = \mathbf{T}\mathbf{z}_k, \tag{1}$$

where $\mathbf{T}$ is the 6×6 frequency-dependent transfer matrix which is real in absence of damping. It follows that the matrix $\mathbf{T}$ and, more specifically, its invariants summarize all the propagation features of the periodic cell. Due to the spectral properties of the symplectic matrix $\mathbf{T}$ [22], the characteristic equation $\det[\mathbf{T} - \lambda\mathbf{I}] = 0$ reads

$$\lambda^6 + I_1\lambda^5 + I_2\lambda^4 + I_3\lambda^3 + I_2\lambda^2 + I_1\lambda + 1 = 0, \tag{2}$$

where the real coefficients I_1, I_2 and I_3 are the invariants of $\mathbf{T}$. Therefore the reversibility property halves the number of the transfer matrix invariants.

The meaning of the eigenvalues λ_i emerges from the Floquet's theorem [22]: there exist free wave motions (characteristic waves) in which $\mathbf{z}_{k+1} = \lambda_i\mathbf{z}_k$, each associated with an eigenvalue of $\mathbf{T}$. If $|\lambda_i| < 1$ the wave amplitude decays in the positive direction (forward wave), if $|\lambda_i| > 1$ it decays in the negative direction

(backward wave), if $|\lambda_i| = 1$ no attenuation exists in the two directions. As known, because of the reversibility of the coefficients of Eq. (2), should we put that λ_i is an eigenvalue, then λ_i^{-1} is an eigenvalue (called the *adjoint* eigenvalue) too. Therefore, forward and backward waves always exist in pairs and have both the same propagation properties. As a result, three eigenvalues λ_1, λ_2 and λ_3 such that $|\lambda_i| \leqslant 1$ $(i = 1, 2, 3)$, completely define the propagation properties of a three-coupled periodic structure. As shown in literature, previous findings can be restated in terms of the propagation constants μ_i, instead of the eigenvalues λ_i, by defining $\lambda_i = \mathrm{e}^{\mu_i}$. This position maps the unitary circle of the $\mathrm{Re}(\lambda_i)$–$\mathrm{Im}(\lambda_i)$ plane into the left half-space of the $\mathrm{Re}(\mu_i)$–$\mathrm{Im}(\mu_i)$ plane.

To solve (2) it would be convenient to rewrite it in terms of the propagation constant μ. By letting $\lambda = \mathrm{e}^{\mu}$ and multiplying by $\mathrm{e}^{-3\mu}$, Eq. (2) reads

$$(\mathrm{e}^{3\mu} + \mathrm{e}^{-3\mu}) + I_1(\mathrm{e}^{2\mu} + \mathrm{e}^{-2\mu}) + I_2(\mathrm{e}^{\mu} + \mathrm{e}^{-\mu}) + I_3 = 0, \tag{3}$$

which is also written as

$$2\cosh 3\mu + 2I_1 \cosh 2\mu + 2I_2 \cosh \mu + I_3 = 0. \tag{4}$$

After some algebraic manipulation the latter equation can be expressed as a cubic equation in $\cosh \mu$ as follows:

$$\cosh^3 \mu + \tfrac{1}{2} I_1 \cosh^2 \mu + \tfrac{1}{4}(I_2 - 3) \cosh \mu + \tfrac{1}{8}(I_3 - 2I_1) = 0. \tag{5}$$

To discuss the three roots $F_{1,2,3}$ of Eq. (5) for $\cosh \mu$, the cases $F_{1,2,3} \in \mathbb{R}$ and $F_{1,2,3} \in \mathbb{C}$ are separately considered. As far as $F_{1,2,3} \in \mathbb{R}$, if $F_{1,2,3} \in \mathscr{I} := [-1, 1]$, then $\mu = \mathrm{i}\vartheta$ and $\lambda = \mathrm{e}^{\mathrm{i}\vartheta}$ is complex with unit modulus; if $F_{1,2,3} \notin \mathscr{I}$, $\mu = \alpha + \mathrm{i}j\pi$ with j integer, and $\lambda = \pm\mathrm{e}^{\alpha}$ is real. Differently, if $F_{1,2,3} \in \mathbb{C}$, $\mu = \alpha + \mathrm{i}\vartheta$ and $\lambda = \mathrm{e}^{\alpha+\mathrm{i}\vartheta}$ is complex with modulus different from 1. The possible location of the eigenvalues on the complex plane are summarized in Fig. 1. The wave propagation characteristics of three-coupled periodic structures can be properly described through a geometric representation on the space of the invariants I_1–I_2–I_3 (Fig. 2). When $\cosh \mu = \mp 1$, two surfaces are obtained in the I_1–I_2–I_3 space given, respectively, by

$$R := \{(I_1, I_2, I_3) | 2 - 2I_1 + 2I_2 - I_3 = 0\},$$

$$S := \{(I_1, I_2, I_3) | 2 + 2I_1 + 2I_2 + I_3 = 0\}. \tag{6}$$

Further surfaces, dividing the real roots of Eq. (5) from the complex ones, are given by

$$P_{1,2} := \{(I_1, I_2, I_3) | 27I_1 - 27I_3 - 2I_1^3 \pm 2\sqrt{(9 + I_1^2 - 3I_2)^3} + 9I_1 I_2 = 0\}. \tag{7}$$

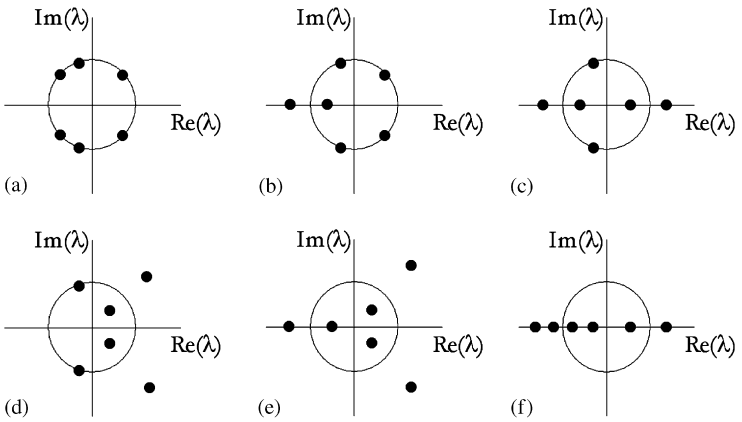

Fig. 1. Transfer matrix eigenvalues scenarios: (a) pass–pass–pass; (b) pass–pass–stop; (c) pass–stop–stop; (d) complex-pass; (e) complex-stop; (f) stop–stop–stop.

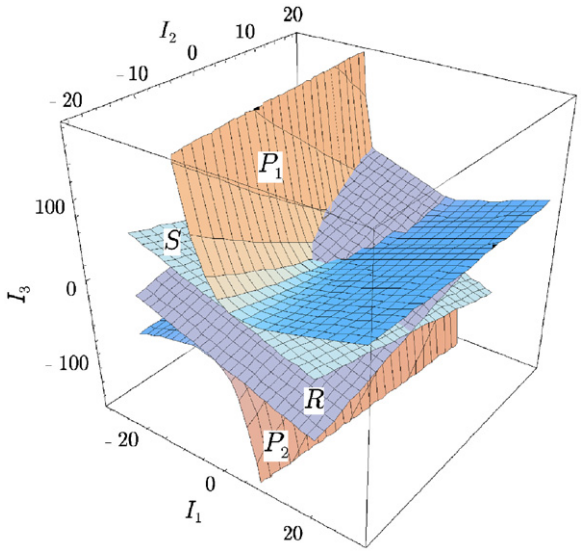

Fig. 2. Propagation zones displayed in the space (I_1, I_2, I_3) of the invariants.

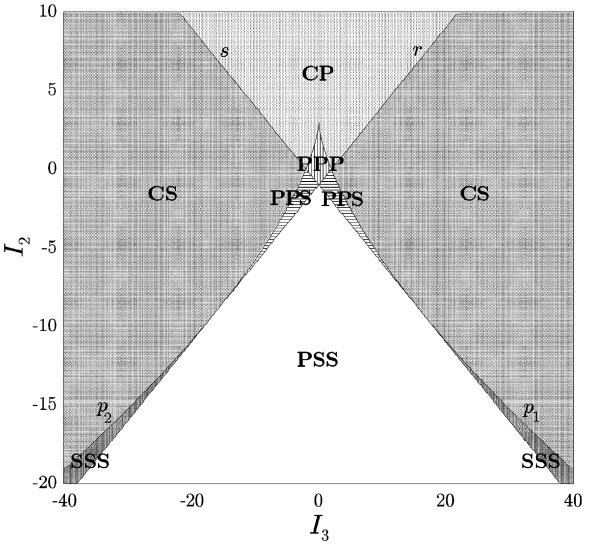

Fig. 3. Propagation zones displayed in the plane (I_3, I_2) of the invariants for $I_1 = 0$.

The four surfaces R, S and $P_{1,2}$ divide the space of the invariants in domains (propagation zones) where the eigenvalues do not differ in type. In Fig. 3 the section $I_1 = 0$ of the space of the invariants is shown, where the curves r, s, $p_{1,2}$ represent the traces of the matching surfaces on the chosen plane; the propagation zones are labeled according to the notation commonly used in literature. As well known [5], such eigenvalues govern the stationary wave transmission properties: if the eigenvalues lie on the unit circle, then free waves propagate harmonically without attenuation (pass band, P); if the eigenvalues are real, then free waves decay without oscillations (stop band, S); furthermore, if the coupling coordinates are more than one, pairs of complex conjugate eigenvalues with modulus different from 1 can exist and harmonic propagation with attenuation of the characteristic waves takes place (complex-band, C). Accordingly, the region where the three pairs of λ lay all on the unit circle is referred to as *pass–pass–pass* (PPP); the regions where two pairs of λ lay on the unit circle while the other pair is real are referred to as *pass–pass–stop* (PPS); the regions where one pair lays on the unit circle while the remaining two pairs of λ are real are referred to as *pass–stop–stop* (PSS); the regions

where only real pairs of eigenvalues occurs are the *stop–stop–stop* (SSS) domains. Moreover, the curves $p_{1,2}$ bound the regions characterized by a pair of complex conjugate eigenvalues and the remaining pair is either real, *complex-stop* (CS), or lays on the unit circle, *complex-pass* (CP). It is worth noticing that only the PPP and PPS regions, unlike the remaining domains, are bounded.

3. Mechanical models transfer matrix derivation

The three-coupled nature of the mechanical models that will be considered in the following sections results from the *sum* of mono-coupled and bi-coupled dynamics. The relevant equations of motion are indeed characterized by the coupling between either a longitudinal or a torsional (mono-coupled) dynamics and a transversal (bi-coupled) one. In order to derive the single-element transfer matrix, it is essential to detect the end forces given the end displacements. This implies the solution of a boundary-value problem of the form

$$\begin{aligned} &\mathscr{M}\ddot{\mathbf{u}} + \mathscr{L}\mathbf{u} = \mathbf{0} \quad \text{in } \mathscr{B}, \\ &\mathscr{K}_H\mathbf{u} = \mathbf{d}_H \qquad \text{on } \partial\mathscr{B}_H \ H = L, R, \end{aligned} \tag{8}$$

where Eq. (8_1) are the field equations defined over the domain $\mathscr{B}$, representing the single element, and Eq. (8_2) are the kinematic boundary conditions at the left and right element interfaces. The terms $\mathscr{M}$ and $\mathscr{L}$ represent inertial and elastic linear differential operators, respectively, acting over the displacement field $\mathbf{u} = \mathbf{u}(x, t)$, while $\mathscr{K}_H$ is the linear kinematic boundary conditions operator acting on the left $\partial\mathscr{B}_L$ and right $\partial\mathscr{B}_R$ element interfaces. The Eq. (8_1) can be put in the form

$$\begin{bmatrix} \mathscr{M}_{uu} & \mathscr{M}_{uv} \\ \mathscr{M}_{vu} & \mathscr{M}_{vv} \end{bmatrix} \begin{pmatrix} \ddot{u} \\ \ddot{v} \end{pmatrix} + \begin{bmatrix} \mathscr{L}_{uu} & \mathscr{L}_{uv} \\ \mathscr{L}_{vu} & \mathscr{L}_{vv} \end{bmatrix} \begin{pmatrix} u \\ v \end{pmatrix} = \begin{pmatrix} 0 \\ 0 \end{pmatrix} \quad \text{in } \mathscr{B}, \tag{9}$$

where the terms u and v represent the mono-coupled and bi-coupled kinematic variables, respectively. The solution, given by

$$\begin{pmatrix} u \\ v \end{pmatrix} = \begin{pmatrix} a \\ b \end{pmatrix} \mathrm{e}^{\beta x} \mathrm{e}^{\mathrm{i}\Omega t} \tag{10}$$

gives rise to the eigenvalue problem $\mathbf{L}(\beta, \Omega)\,\mathbf{a} = \mathbf{0}$ in $\mathscr{B}$, where

$$\mathbf{L} = \begin{bmatrix} L_{uu}(\beta) - \Omega^2 M_{uu} & L_{uv}(\beta) - \Omega^2 M_{uv} \\ L_{vu}(\beta) - \Omega^2 M_{vu} & L_{vv}(\beta) - \Omega^2 M_{vv} \end{bmatrix}, \quad \mathbf{a} = \begin{pmatrix} a \\ b \end{pmatrix} \tag{11}$$

and the algebraic operators M and L have been introduced. The wavenumbers $\beta_i \ i = 1, \ldots, 6$ can be determined by solving the characteristic equation:

$$\beta^6 + J_1\beta^4 + J_2\beta^2 + J_3 = 0, \tag{12}$$

where $J_i = J_i(\Omega)$ $(i = 1, 2, 3)$. Since Eq. (12) admits six roots, the general solution can be written as

$$\begin{pmatrix} u \\ v \end{pmatrix} = \sum_{k=1}^{6} c_k \begin{pmatrix} a_k \\ b_k \end{pmatrix} \mathrm{e}^{\beta_k x} \mathrm{e}^{\mathrm{i}\Omega t}, \tag{13}$$

where the coefficients a_k, b_k are grouped as follows:

$$\begin{aligned} a_k &= L_{uv}(\beta_k) - \Omega^2 M_{uv}, \\ b_k &= \Omega^2 M_{uu} - L_{uu}(\beta_k), \end{aligned} \quad k = 1, 2;$$

$$\begin{aligned} a_k &= \Omega^2 M_{vv} - L_{vv}(\beta_k), \\ b_k &= L_{vu}(\beta_k) - \Omega^2 M_{vu}, \end{aligned} \quad k = 3, 4, 5, 6, \tag{14}$$

so that the eigenvalue problem for uncoupled cases can still be solved. By substituting Eq. (13) into Eq. (8_2) and solving for c_k, the linear homogeneous functions $\mathbf{u}$ over $\mathbf{d}_H$ are obtained. By imposing the equilibrium at

the interfaces through the dynamic boundary conditions:

$$\mathscr{D}_H \mathbf{u} = \mathbf{f}_H \quad \text{on} \quad \partial\mathscr{B}_H \; H = L, R \tag{15}$$

the end forces can be determined as

$$\begin{bmatrix} \mathbf{Z}_{LL} & \mathbf{Z}_{LR} \\ \mathbf{Z}_{RL} & \mathbf{Z}_{RR} \end{bmatrix} \begin{pmatrix} \mathbf{d}_L \\ \mathbf{d}_R \end{pmatrix} = \begin{pmatrix} \mathbf{f}_L \\ \mathbf{f}_R \end{pmatrix}. \tag{16}$$

In Eq. (16) the matrix $\mathbf{Z} = [\mathbf{Z}_{HK}]$, with $H, K = L, R$, represents the frequency-dependent dynamic stiffness matrix, where L and R refers to left and right side of the modular element, respectively. The transfer matrix $\mathbf{T}$, which relates the right end displacements and forces to the left ones, is eventually obtained as

$$\begin{pmatrix} \mathbf{d}_R \\ \mathbf{f}_R \end{pmatrix} = \begin{bmatrix} \mathbf{T}_{dd} & \mathbf{T}_{df} \\ -\mathbf{T}_{fd} & -\mathbf{T}_{ff} \end{bmatrix} \begin{pmatrix} \mathbf{d}_L \\ \mathbf{f}_L \end{pmatrix} \tag{17}$$

by using the well-known relations [23]:

$$\mathbf{T}_{dd} = -\mathbf{Z}_{LR}^{-1}\mathbf{Z}_{LL}, \mathbf{T}_{df} = \mathbf{Z}_{LR}^{-1}, \mathbf{T}_{fd} = -\mathbf{Z}_{RL} + \mathbf{Z}_{RR}\mathbf{Z}_{LR}^{-1}\mathbf{Z}_{LL}, \mathbf{T}_{ff} = -\mathbf{Z}_{RR}\mathbf{Z}_{LR}^{-1}. \tag{18}$$

Once the transfer matrix is obtained, its invariants can be expressed in terms of physical parameters; then, the traces of the surfaces given by Eqs. (6) and (7) can be mapped into a plane of two control parameters duly selected. Among them, the frequency is the most significant one and is always selected so that the curves r, s, and $p_{1,2}$ provide the bounding frequencies of the propagation regions.

As singled out by Mead [1], if the interest lies in the mechanical interpretation of the bounding frequency of multi-coupled periodic structures, it is then crucial to distinguish between two types of coupling coordinates. When symmetric structural elements vibrate in a symmetric mode, some of the matching pairs of coupling coordinates at either end have the same sign and magnitude (*type (i) coordinates*) whereas the remaining pairs have opposite sign and equal magnitude (*type (ii) coordinates*). The opposite occurs for anti-symmetric modes. For periodic structures of symmetric multi-coupled elements, the bounding frequencies of the wave propagation zones are identical to the natural frequencies of a single element with the two types of coupling coordinate either locked or free. In the following sections type (i) and type (ii) coordinates of each three-coupled mechanical model discussed will be identified and the relationship between bounding and natural frequencies will be shown to obey to Mead's results.

4. Periodic axisymmetric cylindrical shells

The general derivation of the propagation regions for three-coupled structures is specialized in this section to deal with periodic pipes sketched in Fig. 4. The pipes are modeled as thin cylindrical shells undergoing axisymmetric (*breathing*) modes of vibration and the periodicity is provided by evenly spaced stiffeners. The displacement field is defined by the longitudinal and transverse components $u(x)$ and $v(x)$, respectively, and by a rotation $\varphi(x) = v'(x)$, x being the abscissa. The parameters that are involved in the model are the following: Young modulus E, Poisson coefficient ν, shell thickness s, mass density ρ, radius r and element length l.

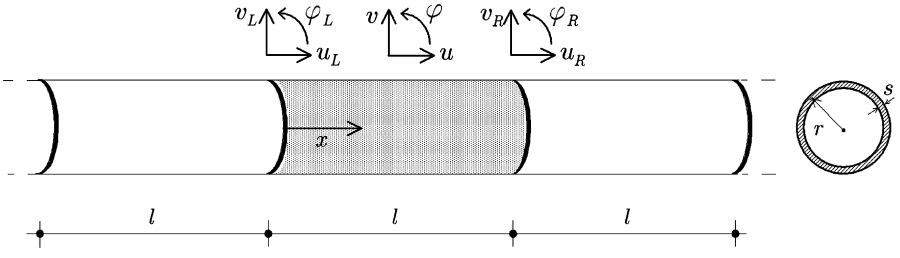

Fig. 4. Periodic cylindrical shells.

Introducing the nondimensional quantities

$$\hat{x} = \frac{x}{r}, \quad \hat{u} = \frac{u}{r}, \quad \hat{v} = \frac{v}{r}, \quad \sigma = \frac{s}{r}, \quad \ell = \frac{l}{r}, \quad \tau = \omega t, \tag{19}$$

where $\omega^2 = E/[\rho r^2(1-\nu^2)]$, the field equations can be written, omitting the hat, as

$$\ddot{u} - u'' - \nu v' = 0, \quad \ddot{v} + \frac{\sigma^2}{12} v'''' + v + \nu u' = 0. \tag{20}$$

In view of the propagation properties analysis that follows on, it is worth stressing that, as shown by the Eq. (20), the coupling between longitudinal and transversal dynamics is governed by the Poisson ratio ν. Moreover, v represents the type (i) coordinate while u and φ are type (ii) coordinates. The kinematic boundary conditions are:

$$u(0) = u_L, \quad u(\ell) = u_R, \quad v(0) = v_L, \quad v(\ell) = v_R, \quad v'(0) = \varphi_L, \quad v'(\ell) = \varphi_R. \tag{21}$$

By defining the equivalent axial and transversal stiffnesses provided by the circumferential stiffeners at the ends of the single element as $k_u/2$ and $k_v/2$, respectively, and setting

$$\begin{aligned} &n_{L,R} = \frac{1-\nu^2}{Es} N_{L,R}, \quad q_{L,R} = \frac{12(1-\nu^2)r^2}{Es^3} Q_{L,R}, \quad m_{L,R} = \frac{12(1-\nu^2)r}{Es^3} M_{L,R}, \\ &\kappa_u = \frac{1-\nu^2}{\sigma} \frac{k_u}{2E}, \quad \kappa_v = \frac{6(1-\nu^2)}{\sigma^3} \frac{k_v}{E}, \end{aligned} \tag{22}$$

the dynamic boundary conditions are given by

$$[u' + \nu v \mp \kappa_u u]_{0,\ell} = \mp n_{L,R}, \quad [-v''' \mp \kappa_v v]_{0,\ell} = \mp q_{L,R}, \quad v''_{0,\ell} = \mp m_{L,R}. \tag{23}$$

Therefore, in order to derive the element transfer matrix according to the procedure set forth in Section 2, the matrix $\mathbf{L}$ in Eq. (11) becomes

$$\mathbf{L} = \begin{bmatrix} -\beta^2 - \Omega^2 & -\nu\beta \\ \nu\beta & 1 + \dfrac{\sigma^2}{12}\beta^4 - \Omega^2 \end{bmatrix}. \tag{24}$$

Starting from the eigenvalue problem governed by the matrix (24), the element transfer matrix is obtained and the invariants are expressed in terms of the physical parameters. The propagation regions are mapped into planes of two control parameters where the curves r, s, $p_{1,2}$ in Fig. 3 give rise to a number of branches. The selected parameter relevant to the results shown in Figs. 5 and 6 are $\ell = 2.0$, $\sigma = 0.1$ and $\kappa_u = 50.0$.

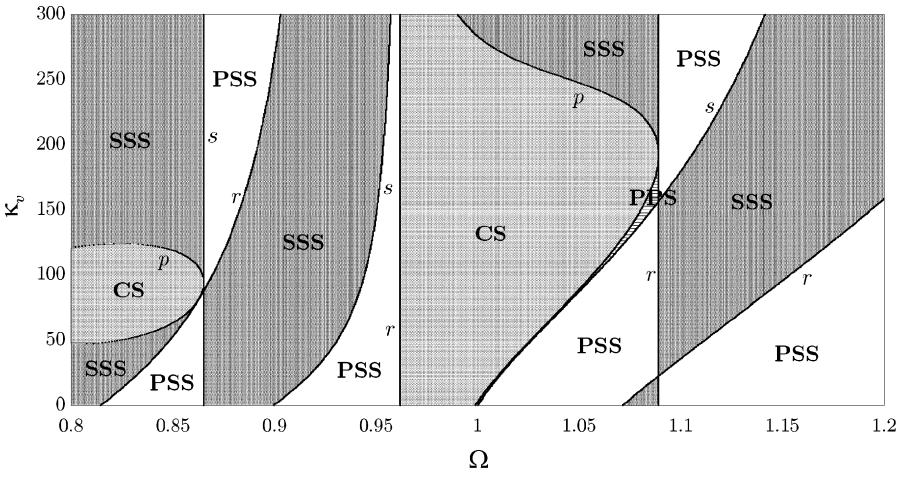

Fig. 5. Propagation zones on the Ω–κ_v plane for $\nu = 0.5$.

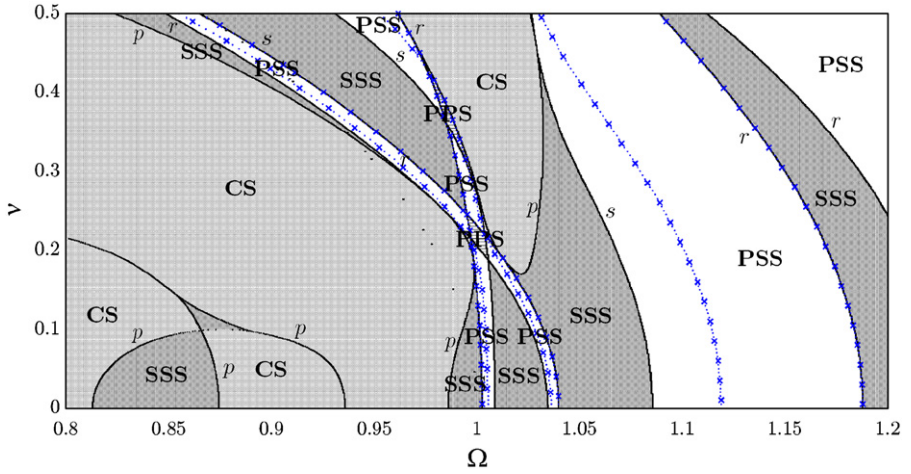

Fig. 6. Propagation zones on the Ω–v plane for $\kappa_u = \kappa_v = 50.0$.

In the limit case $v = 0$, the longitudinal and transversal dynamics are uncoupled so that the resulting propagation scenario can be interpreted as the superposition of the mono-coupled (bar) and the bi-coupled (beam on elastic foundations) scenarios. On the one hand, in the mono-coupled problem, the propagation regions can be either pass (P) or stop (S) and the curves bounding the pass regions, where the eigenvalues lie on the unit circle, can be readily determined by the condition $|\mathrm{tr}(\mathbf{T})| = 2$. This condition applied to the transfer matrix associated to Eq. (20) with $v = 0$ and $\kappa_u = 0.0$, leads to $2\cos\Omega\ell = 2$, so that, for the bar, the longitudinal waves are always in a pass band, regardless of the value of Ω. On the other, the bi-coupled problem of the beam on elastic foundation resting on elastic translational supports behaves qualitatively like the Euler beam on elastic supports studied in Ref. [16]. Thus, the overall propagation scenario is characterized by the superposition of the beam propagation regions, starting from the cut-on frequency ($\Omega > 1$) [18], and the everywhere pass region of the bar. In Fig. 5 the propagation zones are shown on the $\Omega - \kappa_v$ plane for $v = 0.5$ and $\kappa_u = 50.0$; the propagation regions representation obeys the three-coupled nature of the problem, as proven by the appearance of SSS and CS regions. Fig. 6 shows the propagation regions in the $\Omega - v$ plane, for $\kappa_u = \kappa_v = 50.0$. Thus, the evolution of the propagation scenario as the coupling parameter v varies in the range $0.0 \leqslant v \leqslant 0.5$, for given κ_u and κ_v, can be analyzed. As expected, when transversal and longitudinal dynamics are uncoupled ($v = 0$), the flexural natural frequencies of the hinged–hinged single beam, given by $\Omega_n = [1 + (n\pi/\ell)^4\sigma^2/12]^{1/2}$, correspond to bounding frequencies provided by either the branches r or s, namely $\Omega_1 = 1.0025$ (r), $\Omega_2 = 1.0398$ (s), $\Omega_3 = 1.1878$ (r). Moreover, the remaining branches of the same curves correspond to the sliding–sliding single-beam natural frequencies and they tend asymptotically to the fixed–fixed case when $\kappa_v \to \infty$. The natural frequencies of either the free–free or fixed–fixed single bar are not displayed since they are located at higher values of Ω (i.e. $\Omega_n = n\pi/\ell$). As the coupling rises ($v \neq 0$) the three-coupled dynamics forces the bounding frequencies and the associated natural frequencies to bend. For example, the first three natural frequencies of the hinged–hinged single element decrease implying a "softening" effect of the coupling parameter. In particular, the first natural frequency decreases to the value $\Omega_1 = 0.8994$, the second to $\Omega_2 = 0.8143$ while the third to $\Omega_3 = 1.1116$; the crossing between the first and second natural frequency occurs at $v = 0.25$. The crossed curves in Fig. 6 represent the first six natural frequencies of the two element periodic pipe when v (type (i) coordinate) is locked while u and φ (type (ii) coordinates) are free. Their paths on the Ω–v plane are always within either a PSS or a PPS region. As the periodic structure consists of two elements, two natural frequencies are found in each PSS region. Moreover, as expected, for each pair, one natural frequency overlaps with a bounding frequency provided by either r or s branches; for low values of v ($v < 0.25$) such overlapping occurs according to the alternating sequence: r, s, r.

5. Periodic symmetric thin-walled beams

Thin-walled beams with symmetric cross-section undergoing flexural–torsional oscillations are analyzed in this section (see Fig. 7a). The flexural–center axis is taken as the x-axis and the distance between the flexural

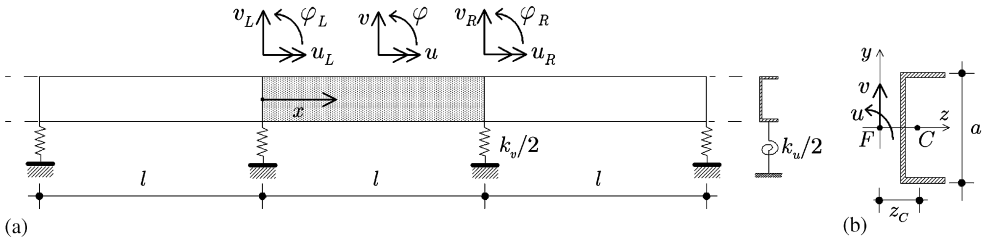

Fig. 7. Periodic thin-walled beam: (a) beam element displacement field and (b) beam cross-section.

center F and the centroid C is equal to z_C, as sketched in Fig. 7b. The displacement field is defined by the torsional rotation $u(x)$, transverse component $v(x)$, and by the flexural rotation $\varphi(x) = v'(x)$. The parameters entering the models are: mass density ρ, cross-section area A, polar moment of inertia I_G ($I_F = I_G + Az_C^2$), Young modulus E, moment of inertia $I = I_z$, tangential elastic modulus G and torsional inertia J. Introducing the nondimensional quantities

$$\hat{x} = \frac{x}{a}, \quad \hat{v} = \frac{v}{a}, \quad \alpha = \frac{Aa^2}{I_F}, \quad \gamma = \frac{\alpha GJ}{EI}, \quad \ell = \frac{l}{a}, \quad \sigma = \frac{z_C}{a}, \quad \tau = \omega t, \tag{25}$$

where $\omega^2 = EI/(\rho Aa^4)$, the field equations read, omitting the hat, as

$$\ddot{u} - \alpha\sigma\ddot{v} - \gamma u'' = 0, \quad \ddot{v} - \sigma\ddot{u} + v'''' = 0, \tag{26}$$

where the warping torsional stiffness was neglected. In this case, it is worth pinpointing that, as shown by Eq. (26), the coupling between torsional and transversal dynamics is governed by inertia terms through the parameter σ. For this model φ represents the type (i) coordinate while u and v are type (ii) coordinates. The kinematic boundary conditions are still given by the expressions (21) and by setting

$$q_{L,R} = \frac{Q_{L,R}a^2}{EI}, \quad t_{L,R} = \frac{T_{L,R}a}{GJ}, \quad m_{L,R} = \frac{M_{L,R}a}{EI}, \quad \kappa_u = \frac{k_u a}{GJ}, \quad \kappa_v = \frac{k_v a^3}{EI}, \tag{27}$$

where k_u and k_v represent the rotational and transversal spring stiffnesses, the dynamic boundary conditions are:

$$[u' \mp \kappa_u u]_{0,\ell} = \mp t_{L,R}, \quad [-v''' \mp \kappa_v v]_{0,\ell} = \mp q_{L,R}, \quad v''_{0,\ell} = \mp m_{L,R}. \tag{28}$$

Therefore, in order to derive the element transfer matrix according to the procedure described in Section 2, the matrix $\mathbf{L}$ in Eq. (11) becomes

$$\mathbf{L} = \begin{bmatrix} -\gamma\beta^2 - \Omega^2 & \sigma\alpha\Omega^2 \\ \sigma\Omega^2 & \beta^4 - \Omega^2 \end{bmatrix}. \tag{29}$$

Starting from the eigenvalue problem governed by the matrix (29), the element transfer matrix is obtained and the invariants are expressed in terms of physical parameters. The selected parameter relevant to the results shown in Figs. 8 and 9 are $\ell = 5.0$, $\alpha = 1.0$ and $\gamma = 2.0$. In the $\sigma = 0.0$ borderline case the torsional and transversal dynamics are uncoupled. Here, we can make the same remarks as in the case of pipes mentioned above. In Fig. 8 the propagation zones are shown on the Ω–κ_v plane for $\sigma = 2.0$ and $\kappa_u = 6.0$. Fig. 9 shows the propagation regions in the Ω–σ plane, for $\kappa_u = 6.0$ and $\kappa_v = 2.0$. Thus, the evolution of the propagation scenario as the coupling parameter σ varies in the range between $0.0 \leqslant \sigma \leqslant 2.0$, can be analyzed. For $\sigma = 0.0$ the flexural natural frequencies of the hinged–hinged single beam, $\Omega_n = (n\pi/\ell)^2$, correspond to the bounding frequencies given by the branches of curves r and s, such as $\Omega_1 = 0.395$ (r), $\Omega_2 = 1.579$ (s). The natural frequencies of the free–free (fixed–fixed) single bar ($\Omega_n = \sqrt{\gamma}n\pi/\ell$) also correspond to branches of curves r and s; the first two of them are located at $\Omega_1 = 0.888$ (r) and $\Omega_2 = 1.777$ (s). Moreover, the remaining branches of the same curves correspond to the sliding–sliding single-beam natural frequencies. As noticed in the previous model, as the coupling parameter σ increases, the above-mentioned uncoupled natural frequencies of the single element move along the r and s branches giving rise to involved paths. The lower natural frequencies of the periodic thin-walled beam composed by two elements when φ (type (i) coordinate) is locked while u and v

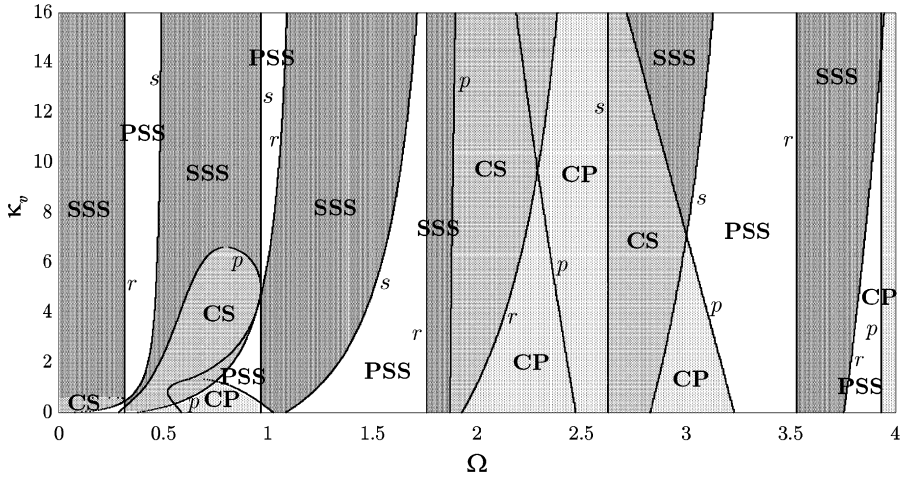

Fig. 8. Propagation zones on the Ω–κ_v plane for $\sigma = 2.0$.

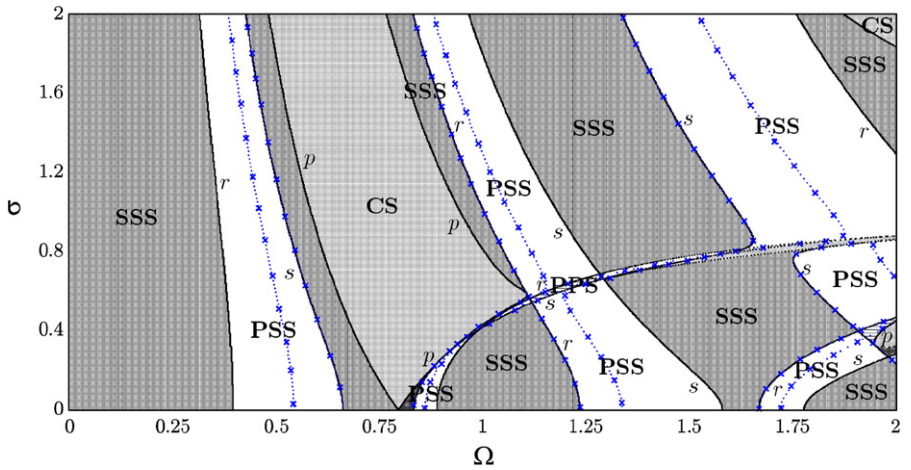

Fig. 9. Propagation zones on the Ω–σ plane for $\kappa_u = 6.0$ and $\kappa_v = 2.0$.

(type (ii) coordinates) are free are represented in Fig. 9 by the crossed curves. As expected such natural frequencies are forbidden within either SSS or CS regions. Since the periodic system is composed by two elements, two natural frequencies are found in each PSS region. Moreover, for each pair, one natural frequency overlaps with a bounding frequency provided by either r or s branches. In this case, crossing and veering phenomena in both bounding and natural frequencies can be observed around $\Omega = 1.2$ and 1.8.

6. Periodic equivalent truss beams

A truss beam structure is chosen as a three-coupled periodic mechanical model in this section as sketched in Fig. 10. Hence, it is worth distinguishing between a *local* periodicity due to the single truss module and a *global* periodicity due to evenly spaced elastic supports (see Fig. 10a). By assuming $h_m/l \gg 1$ and a large number of truss modules between the supports and being mainly interested to the global dynamic behavior, an equivalent continuum model, sketched in Fig. 10b, can be derived through a homogenization technique based on the single-truss module properties (see Fig. 11). The slenderness of the single-truss beam span entails high-frequency shear modes; by neglecting these modes a course shear indeformable continuum beam model is assumed. By labeling A_b, A_t, A_d the areas of the bottom, top and diagonal bars, respectively, and with l_m and

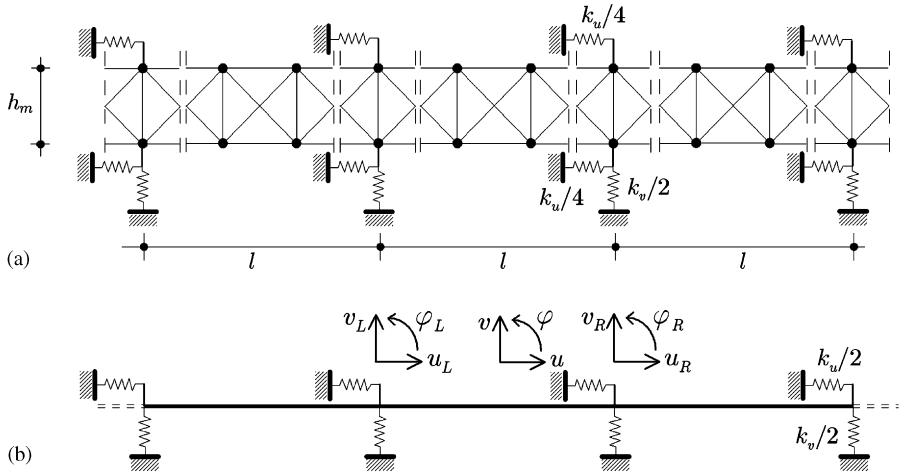

Fig. 10. Periodic equivalent truss beam: (a) periodic truss beam and (b) equivalent continuum model.

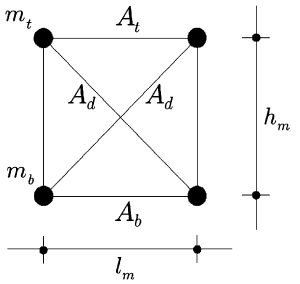

Fig. 11. Truss beam module.

h_m the module width and height, respectively, and also with m_t and m_b the top and bottom nodal masses, respectively, and setting

$$A_t = (1+t)A_b, \quad A_d = (1+d)A_b, \quad m_t = (1+m)m_b, \quad h_m = (1+h)l_m, \tag{30}$$

the equivalent continuum model constitutive law can be expressed [19], for the restoring elastic forces, as

$$N = EA_b(\xi u' - \zeta_e l_m v''), \quad M = EA_b(-\zeta_e l_m u' + \eta l_m^2 v'') \tag{31}$$

and for the inertial masses as

$$m_{uu} = m_{vv} = \frac{(2+m)m_b}{l_m}, \quad m_{u\phi} = m_{\phi u} = -\frac{1}{2}m\,m_b(1+h),$$
$$m_{\phi\phi} = \frac{1}{4}(2+m)(1+h)^2 m_b\, l_m, \tag{32}$$

where the equivalent beam axis has been located at the mid-height of the truss beam and the axial deformation and bending curvature are introduced according to the Euler–Bernoulli beam model. By setting

$H = h^2 + 2h + 2$, the parameters entering Eqs. (31) and (32) are defined as

$$\xi = (2+t) + 2(1+d)H^{-3/2}, \quad \eta = \frac{1}{4}(h+1)^2(t+2), \quad \zeta_e = \frac{1}{2}(1+h)t,$$
$$\zeta_i = \frac{1}{2}\frac{(1+h)m}{2+m}, \quad \mu = \frac{1}{4}(1+h)^2. \tag{33}$$

By introducing the nondimensional quantities

$$\hat{x} = \frac{x}{l_m}, \quad \hat{u} = \frac{u}{l_m}, \quad \hat{v} = \frac{v}{l_m}, \quad \ell = \frac{l}{l_m}, \quad \tau = \omega t, \tag{34}$$

where $\omega^2 = EA_b/[m_b l_m(2+m)]$, the field equations become

$$\ddot{u} - \zeta_i \ddot{v}' - \xi u'' + \zeta_e v''' = 0, \quad \ddot{v} - \mu \ddot{v}'' + \zeta_i \ddot{u}' + \eta v'''' - \zeta_e u''' = 0. \tag{35}$$

As shown by Eq. (35), the coupling between longitudinal and transversal dynamics is governed by the parameters ζ_α, $\alpha = e, i$ defined in Eq. ($33_{3,4}$), respectively. Moreover, v represents the type (i) coordinate while u and φ are type (ii) coordinates.

The kinematic boundary conditions are once more given by the expressions (21); furthermore, by putting

$$n_{L,R} = \frac{N_{L,R}}{EA_b}, \quad q_{L,R} = \frac{Q_{L,R}}{EA_b}, \quad m_{L,R} = \frac{M_{L,R}}{EA_b l_m}, \quad \kappa_{u,v} = \frac{k_{u,v}\, l_m}{2EA_b}, \tag{36}$$

where $k_u/2$ and $k_v/2$ represent the stiffness of evenly spaced longitudinal and transversal elastic supports (Fig. 10b), respectively, the dynamic boundary conditions become

$$[\xi u' - \zeta_e v'' \mp \kappa_u u]_{0,\ell} = \mp n_{L,R},$$
$$[\zeta_e u'' - \eta v''' + \mu \ddot{v}' - \zeta_i \ddot{u} \mp \kappa_v v]_{0,\ell} = \mp q_{L,R},$$
$$[\eta v'' - \zeta_e u']_{0,\ell} = \mp m_{L,R}. \tag{37}$$

In this case the derivation of the element transfer matrix outlined in Section 2 starts by the matrix $\mathbf{L}$ in Eq. (11) taking the form

$$\mathbf{L} = \begin{bmatrix} -(\xi\beta^2 + \Omega^2) & \beta(\Omega^2\zeta_i + \beta^2\zeta_e) \\ -\beta(\Omega^2\zeta_i + \beta^2\zeta_e) & \eta\beta^4 + \Omega^2(\mu\beta^2 - 1) \end{bmatrix}. \tag{38}$$

Then, along the line followed in the previous section, the transfer matrix invariants are obtained in terms of the physical parameters in order to map the surfaces (6) and (7).

The selected parameter relevant to the results shown in Figs. 9 and 10 are $\xi = 2.0$, $\zeta_i = 0.0$, $\mu = 0.25$, $\ell = 5.0$, $\eta = 0.5$ and $\kappa_u = 2.0$. Therefore in the present analysis the inertial coupling is absent.

In the uncoupled case ($\zeta_e = 0.0$) the mono-coupled longitudinal dynamics of the bar behaves like in the first case, giving rise to a pass region for every frequency for $\kappa_u = 0.0$, while the bi-coupled transversal one coincides with the Euler beam resting on elastic supports [16]. The representation of the propagation regions on the Ω–κ_v plane for $\zeta_e = 0.5$ is provided by Fig. 12. As expected, the nonzero coupling parameter activates the three-coupled dynamics and the relevant propagation scenario becomes more involved, including SSS and CS regions.

The evolution from the uncoupled to the coupled dynamics in terms of propagation zones can be better explained by referring to the Ω–ζ_e plane as done in Fig. 13 for $\kappa_v = 1.0$ and $\kappa_u = 2.0$. When $\zeta_e = 0$ the bounding frequencies given by branches of curves r and s are found at the hinged–hinged single-beam natural frequencies, given by $\Omega_n = [(n\pi/\ell)^4\eta]^{1/2}$; the first three of them are found at $\Omega_1 = 0.279$ (r), $\Omega_2 = 1.117$ (s), $\Omega_3 = 2.512$ (r). The birth of free–free (or fixed–fixed) single-bar longitudinal natural frequencies can also be observed, namely $\Omega_n = [(n\pi/\ell)^2\xi]^{1/2}$; the first three of them can be found at $\Omega_1 = 0.888$ (r), $\Omega_2 = 1.777$ (s) and $\Omega_3 = 2.666$ (r). The crossed curves in Fig. 13 represent the first six natural frequencies of the periodic equivalent truss beam composed by two elements when v (type (i) coordinate) is free while u and φ (type (ii) coordinates) are locked. Their paths on the Ω–ζ_e plane are always within either a PSS or a PPS region. Since

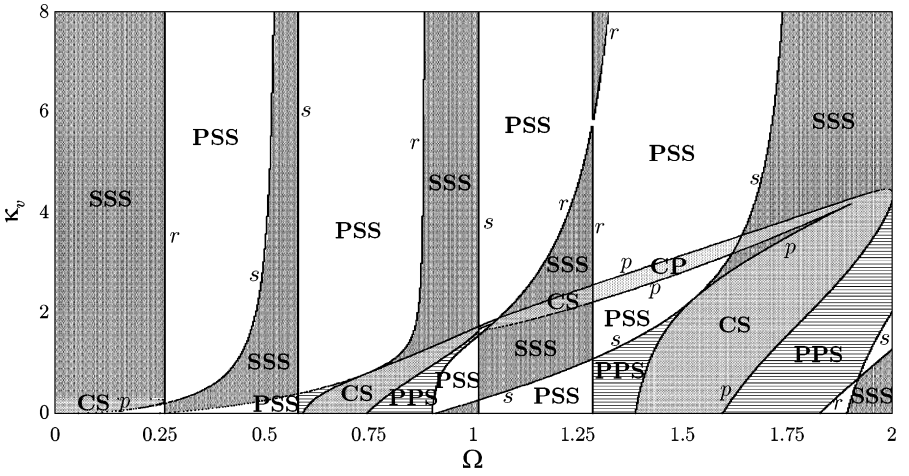

Fig. 12. Propagation zones on the Ω–κ_v plane for $\zeta_e = 0.5$.

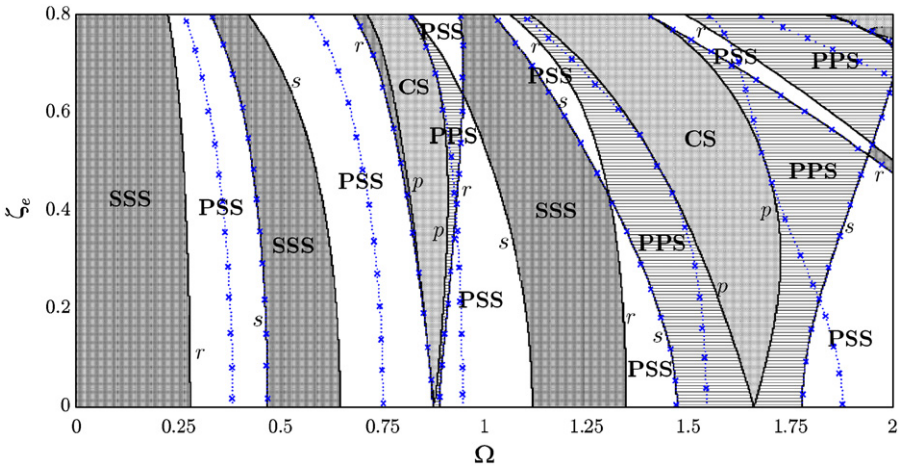

Fig. 13. Propagation zones on the Ω–ζ_e plane for $\kappa_v = 1.0$ and $\kappa_u = 2.0$.

the periodic system is composed by two elements, two natural frequencies are found in each PSS region. Moreover, as expected, for each pair, one natural frequency overlaps with a bounding frequency provided by either r or s branches. Several crossing phenomena can be observed around $\Omega = 0.9$ and in the range $\Omega = 1.6-2.0$.

7. Conclusions

Starting from the characteristic equation of the symplectic transfer matrix, three-coupled periodic structures were analyzed on the space of the invariants. Such approach helped derive analytically the boundaries of the combined stop, pass and complex domains. Pass–pass–pass and pass–pass–stop bands were both found to be confined to a small neighborhood of the origin. Different paradigmatic mechanical models characterized by constitutive elastic and/or inertial coupling between mono- and bi-coupled dynamics were discussed. Constitutive elastic coupling in stiffened pipes and truss beams, and inertial coupling in thin-walled beam resting on elastic supports, were tackled. Free-wave propagation domains on different physical parameters planes were obtained through nonlinear mappings from the plane of the invariants. Such representation provides the following remarkable insights: (i) a measure of the influence of the coupling parameters on the

interaction between longitudinal or torsional (mono-coupled) and transversal (bi-coupled) dynamics; (ii) the domains where natural frequencies must lie for given boundary conditions; (iii) a tool for predicting crossing and veering phenomena.

Acknowledgment

This work was partially supported under the FY 2003-04 PRIN GRANT; http://www.disg.uniroma1.it/fendis.

References

[1] D.J. Mead, Wave propagation and natural modes in periodic systems: II bi-coupled systems, with and without damping, *Journal of Sound and Vibration* 40 (1975) 19–39.
[2] Y.K. Lin, T.J. McDaniel, Dynamics of beam-type periodic structures, *Journal of Engineering for Industry—Transaction of ASME* (1969) 1133–1141.
[3] G. Sen Gupta, Natural flexural waves and the normal modes of periodically-supported beams and plate, *Journal of Sound and Vibration* 13 (1970) 89–101.
[4] M.G. Faulkner, D.P. Hong, Free vibrations of mono-coupled periodic system, *Journal of Sound and Vibration* 99 (1985) 29–42.
[5] J. Signorelli, A.H. von Flotow, Wave propagation, power flow, and resonance in a truss beam, *Journal of Sound and Vibration* 126 (1988) 127–144.
[6] A.H. von Flotow, Disturbance propagation in structural networks, *Journal of Sound and Vibration* 106 (1986) 433–450.
[7] Y. Yong, Y.K. Lin, Propagation of decaying waves in periodic and piecewise periodic structures of finite length, *Journal of Sound and Vibration* 129 (1989) 99–118.
[8] Y. Yong, Y.K. Lin, Dynamic response of truss-type structural networks: a wave propagation approach, *Journal of Sound and Vibration* 156 (1992) 27–45.
[9] W.J. Chen, C. Pierre, Exact linear dynamics of periodic and disordered truss beams: localization of normal modes and harmonic waves, *Proceedings of 32nd AIAA/ASME/ASCE/AHS/ASC Structures, Structural Dynamics, and Material Conference*, 1991, Baltimore, MD.
[10] C. Pierre, M.P. Castanier, W.J. Chen, Wave localization in multi-coupled periodic structures: application to truss beams, *Applied Mechanics Review* 49 (1996) 65–86.
[11] G.Q. Cai, Y.K. Lin, Wave propagation and scattering in structural networks, *Journal of Engineering Mechanics* 117 (1991) 1555–1574.
[12] R.S. Langley, N.S. Bardell, P.M. Loasby, The optimal design of near-periodic structures to minimize vibration transmission and stress levels, *Journal of Sound and Vibration* 207 (1997) 627–646.
[13] F. Romeo, A. Luongo, Vibration reduction in piecewise bi-coupled periodic structures, *Journal of Sound and Vibration* 268 (2003) 601–615.
[14] W.X. Zhong, F.W. Williams, Wave problems for repetitive structures and symplectic mathematics, *Proceedings of the Institute of Mechanical Engineers Part C* 206 (1992) 371–379.
[15] R.S. Langley, A transfer matrix analysis of the energetics of structural wave motion and harmonic vibration, *Proceedings Royal Society of London A* 452 (1996) 1631–1648.
[16] F. Romeo, A. Luongo, Invariant representation of propagation properties for bi-coupled periodic structures, *Journal of Sound and Vibration* 257 (2002) 869–886.
[17] F. Romeo, A. Paolone, Propagation properties of three-coupled periodic mechanical systems, *Proceedings of 20th ASME Biennial Conference on Mechanical Vibration and Noise*, Paper No. DETC'05/VIB-85617, September 2005, Long Beach, California.
[18] S.V. Sorokin, O.A. Ershova, Plane wave propagation and frequency band gaps in periodic plates and cylindrical shells with and without heavy fluid loading, *Journal of Sound and Vibration* 278 (2004) 501–526.
[19] A. Di Carlo, N. Rizzi, A. Tatone, Continuum modelling of a beam-like latticed truss: identification of the constitutive functions for the contact and inertial actions, *Meccanica* 25 (1990) 168–174.
[20] A.K. Noor, M.S. Anderson, Continuum model for beam- and plate-like lattice structures, *American Institute of Aeronautics and Astronautics Journal* 16 (1978) 1219–1228.
[21] A.K. Noor, Continuum modeling for repetitive lattice structures, *Applied Mechanics Review* 41 (1988) 285–296.
[22] V.I. Arnold, *Mathematical Methods of Classical Mechanics*, Springer, New York, 1978.
[23] E.C. Pestel, F.A. Leckie, *Matrix Methods in Elastomechanics*, McGraw-Hill, New York, 1963.